ACS APPLIED MATERIALS & INTERFACES

Research Article

www.acsami.org

Activation and Enhancement of Room-Temperature Ferromagnetism in Cu-Doped Anatase TiO_2 Films by Bound Magnetic Polaron and Oxygen Defects

Jian-Yun Zheng,[†,‡] Shan-Hu Bao,[†] Yan-Hong Lv,[†,‡] and Ping Jin*[,†,§]

[†]State Key Laboratory of High Performance Ceramics and Superfine Microstructure, Shanghai Institute of Ceramics, Chinese Academy of Sciences, Shanghai 200050, People's Republic of China

[‡]Graduate School of Chinese Academy of Sciences, Beijing 100049, People's Republic of China

[§]National Institute of Advanced Industrial Science and Technology (AIST), Moriyama, Nagoya 463-8560, Japan

Supporting Information

ABSTRACT: Cu-doped anatase TiO_2 films grown by magnetron sputtering at room temperature showed the unexpected observation of room-temperature ferromagnetism, which was enhanced or destroyed corresponding to low or high impurity concentration via vacuum annealing. On the basis of the analysis of composition and structure, the most important factor for activating ferromagnetism can be identified as the creation of grain boundary defects. In addition, oxygen defects can be the dominating factor for increasing the saturation moment of the 0.19 at. % Cu-doped TiO_2 film from 0.564 to 26.41 emu/cm^3. These results help elucidate the origin of ferromagnetism and emphasize the role of oxygen defects for the application of ferromagnetic films.

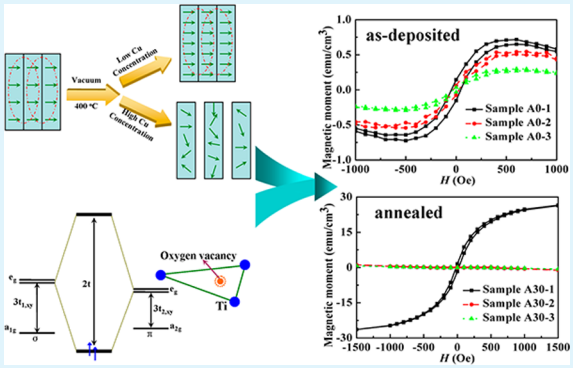

KEYWORDS: *anatase TiO_2 films, Cu-doped, room-temperature ferromagnetism, oxygen defect*

1. INTRODUCTION

Spintronics, or *spin electronics*, refers to an emerging electronic device technology in which the role played by electron (and more generally nuclear) spin in solid state physics is studied, and spin properties instead of or in addition to charge degrees of freedom are exploited. Spintronics has vast potential in the storage, processing, and transmission of digital information, as well as in optical and magnetic sensors.[1,2] Ferromagnetic semiconductors prepared by doping the impurities into host semiconductors are appealing materials for spintronics because these semiconductors are envisioned as producing the low power consumption and great operating speed of spintronics devices.[3,4] Among the materials (mostly III−V and II−VI compounds) so far reported, successful prototype devices have employed the Mn-doped GaAs,[5] ZnSe,[6,7] and InAs[8] diluted magnetic semiconductors (DMSs) to achieve spin polarization. However, these DMSs exhibit the cryogenic Curie temperatures (T_C, ~100 K),[9] which have hindered the development of practical devices. Apparently, it is highly desirable to pursue the DMSs with higher T_C, especially T_C over room temperature.

Since the breakthrough work reported by Matsumoto et al.,[3] magnetic impurity-doped TiO_2 films have attracted considerable attention, owing to the appearance of room-temperature ferromagnetism in this group. With the behaviors of room-temperature ferromagnetism in doped TiO_2 films, several arguments have been proposed by some authors, mainly dividing into three groups. The first group is based on the formation of clusters of magnetic dopants, which principally happen in the doped TiO_2 films with the high concentration of magnetic dopants.[10−13] However, the idea of magnetic clusters is not the mechanism of intrinsic ferromagnetism of TiO_2 based DMSs, and insufficiently explains the presence of room-temperature ferromagnetism in low concentration doped TiO_2 films. The second set of researchers postulate the formation of bound magnetic polarons (BMP) associated with oxygen vacancies in a dielectric matrix with magnetic impurities.[14,15] A special report of ferromagnetism in Co-doped TiO_2 films prepared by direct chemical routes has led to the development of a third class of model.[16] The intrinsic ferromagnetism in this report is thought to arise from grain boundary defects located at nanocrystal fusion interfaces. Unfortunately, as previously described, much of the research focuses on the origin of room-temperature ferromagnetism in magnetic impurities doped TiO_2 films. A drawback to these studies is that the impurities can segregate to yield the magnetic precipitates or clusters that actually influence the intrinsic ferromagnetism of the doped films.[17] Therefore, these issues have motivated some researchers to probe the experiments on nonmagnetic impurities doped TiO_2 such as Cu-doped.[18,19]

Received: September 3, 2014
Accepted: December 1, 2014
Published: December 1, 2014

Table 1. Experimental Conditions and Results of the Cu-Doped TiO_2 Films[a]

sample	P_{Cu} (W)	t_A (min)	C_{Cu} (at. %)	h_f (nm)	M_r (emu/cm^3)	H_c (Oe)	M_s (emu/cm^3)
A0-1	2	0	0.19 ± 0.03	502	0.144	47	0.564
A30-1	2	30	0.19 ± 0.03	502	1.517	19	26.41
A0-2	50	0	4.57 ± 0.45	512	0.063	30	0.441
A30-2	50	30	4.57 ± 0.45	512	—	—	—
A0-3	100	0	19.1 ± 0.60	786	0.036	29	0.240
A30-3	100	30	19.1 ± 0.60	786	—	—	—

[a] P_{Cu}, t_A, C_{Cu}, h_f, M_r, H_c, and M_s are the power of Cu target, annealing time, doping concentration, film thickness, remanent magnetization, intrinsic coercivity, and saturation momen, respectivelyt. The blank is represented as "—".

Cu is a potential magnetic ion with a total spin of 1/2 by Hund's rule,[20] and neither metallic Cu nor its oxide are ferromagnetic. Furthermore, Duhalde et al.[21] have reported that the oxygen defects could play a crucial role for the room-temperature ferromagnetism, and the doping content could also affect the number of oxygen vacancies. Depressingly, the microscopic origins of ferromagnetism in Cu-doped TiO_2 films remain poorly understood. A detailed perception of ferromagnetism in wide-bandgap DMSs is required to harness functionality for device applications. Moreover, the regulation of magnetic moment for the DMSs should be also concerned and investigated so as to satisfy the demands of an application.

In the present work, we design a series of experiments to search the origin and enhancement of room-temperature ferromagnetism in Cu-doped TiO_2 films deposited by direct current reactive magnetron sputtering (DCRMS) at room temperature. These doped TiO_2 films had Cu mole fractions (x at. %) in the range of about 0.19−19.10 at. %. It is easily observed that all the doped TiO_2 films consistently showed weak room-temperature ferromagnetism. After further vacuum annealing at 400 °C, the saturation moment (M_s) of the 0.19 at. % Cu-doped TiO_2 film reached up to ∼26.41 emu/cm^3, which was around 47 times larger than that of the fresh film (∼0.564 emu/cm^3). Nevertheless, the ferromagnetism in other films with higher doping concentration was destroyed by the identical annealing process. With the investigation of film composition and structure, the percolation of BMP between the adjacent grains plays an important role for the activation of ferromagnetism in Cu-doped TiO_2 films. Besides the dependence of ferromagnetism on oxygen defects found here is also discussed in the context of current models.

2. EXPERIMENTAL SECTION

The Cu-doped TiO_2 films with different doping concentration were deposited on n-type Si (100) wafers (the thickness of 0.5 mm) by DCRMS at room temperature. Pure Ti and Cu targets (99.99% purity) were sputtered in Ar (99.99%) and O_2 (99.99%) mixed atmosphere. The deposition was conducted at a deposition pressure of 1.4 Pa, a deposition time of 2 h, a substrate bias of −50 V and a fixed hybrid gas composed of 105 sccm Ar flow rates and 15 sccm O_2 flow rates. Although there was no intentional substrate heating in these experiments, the substrate temperature increased from around 25 to 100 °C during deposition due to the bombardment of energetic particles on the substrate surface. DC power imposing on the Cu target as a variable deposition parameter, which was set as 2 W, 50 and 100 W corresponding to Samples A0-1, A0-2 and A0-3, respectively, was selected to control the doping concentration in Cu-doped TiO_2 films. After film deposition, the fresh films were annealed in vacuum annealing furnace at 400 °C for 30 min. In this work, the films with 0 and 30 min of annealing time are denoted as Sample A0-X and Sample A30-X (X = 1, 2, 3), respectively. Composition, structural and magnetic measurements were made on films both before and after annealing. X-ray photoelectron spectroscopy (XPS) with monochromated Al Kα radiation at pass energy of 29.4 eV was applied to analyze the chemical composition of the film surface. The film structure and crystalline quality were characterized by X-ray diffraction (XRD), field emission scanning electron microscopy (FESEM), and high resolution transmission electron microscopy (HRTEM). Magnetization (M) versus applied magnetic field (H) at 300 K was measured using a Quantum Design superconducting quantum interference device (SQUID) magnetometer. Magnetization data of all Cu-doped TiO_2 films were corrected for diamagnetism of the substrate. Typical net magnetic moments for the TiO_2 films used in this study were on the order of 10^{-6} emu absolute, which should be approximately 2 orders of magnitude larger than the base sensitivity of the SQUID magnetometer. The preparation and characterization of further details for Cu-doped TiO_2 films are described in Supporting Information (SI) S1 and S2, respectively.

3. RESULTS AND DISCUSSION

The partial experimental conditions and outcomes of the Cu-doped TiO_2 films are summarized in Table 1. XPS analyses on all samples show that the TiO_2 films allowed 0.19 at. %, 4.57 at. %, and 19.10 at. % Cu doping, assigned as Samples A0-1 (A30-1), A0-2 (A30-2), and A0-3 (A30-3), respectively. XRD patterns for all samples in Figure 1(i) indicate that the phase composition and crystallinity of the samples depend strongly on both the Cu content and the annealing treatment. All peaks for Samples A0-1 and A30-1 were indexed as a TiO_2 anatase structure, and no secondary phase and metal-related peak were detected within the sensitivity of XRD. However, the peak position of Sample A0-1 was slightly shifted toward lower angle compared to the pure anatase phase.[22] The peak shift could be attributed to the incorporation of Cu ions into the TiO_2 lattice leading to the increment of the film cell parameter c, as reported by other researchers.[23] On the contrary, the peak position of Sample A30-1 presented an evident shift toward higher angle than that of Sample A0-1, which can imply a relaxation of the lattice along the c axis as well as the presence of plentiful of oxygen vacancies in Sample A30-1.[14] These conjectures will be further confirmed by the analysis of XPS mentioned later. Moreover, a comparison of the full width at half-maximum (fwhm) values of (101) peak intensities of Samples A0-1 and A30-1 exhibited a subtle improvement in crystallinity with annealing by a 0.057° decrease in the fwhm value (shown in SI S3)). With the increase of doping concentration, both Samples A0-2 and A0-3 displayed nanocrystalline structure and their peak position moved gradually toward the CuO (−111) peak. When the film growth was performed at room temperature, the diffusion of deposited particles was limited on a narrow range resulting in the substitution of a tiny fraction of Cu ions into the Ti sites and the remanent Cu atoms formed the secondary phase (e.g., copper oxide). On the other hand, the growth of the crystalline grains for Samples A0-2 and A0-3 during the deposition can be suppressed because of the existence of the second phase particles.[24] After annealing at 400 °C for 30 min, Samples A30-2 and A30-3 both had polyphase structure, but their phase composition was different. As shown in

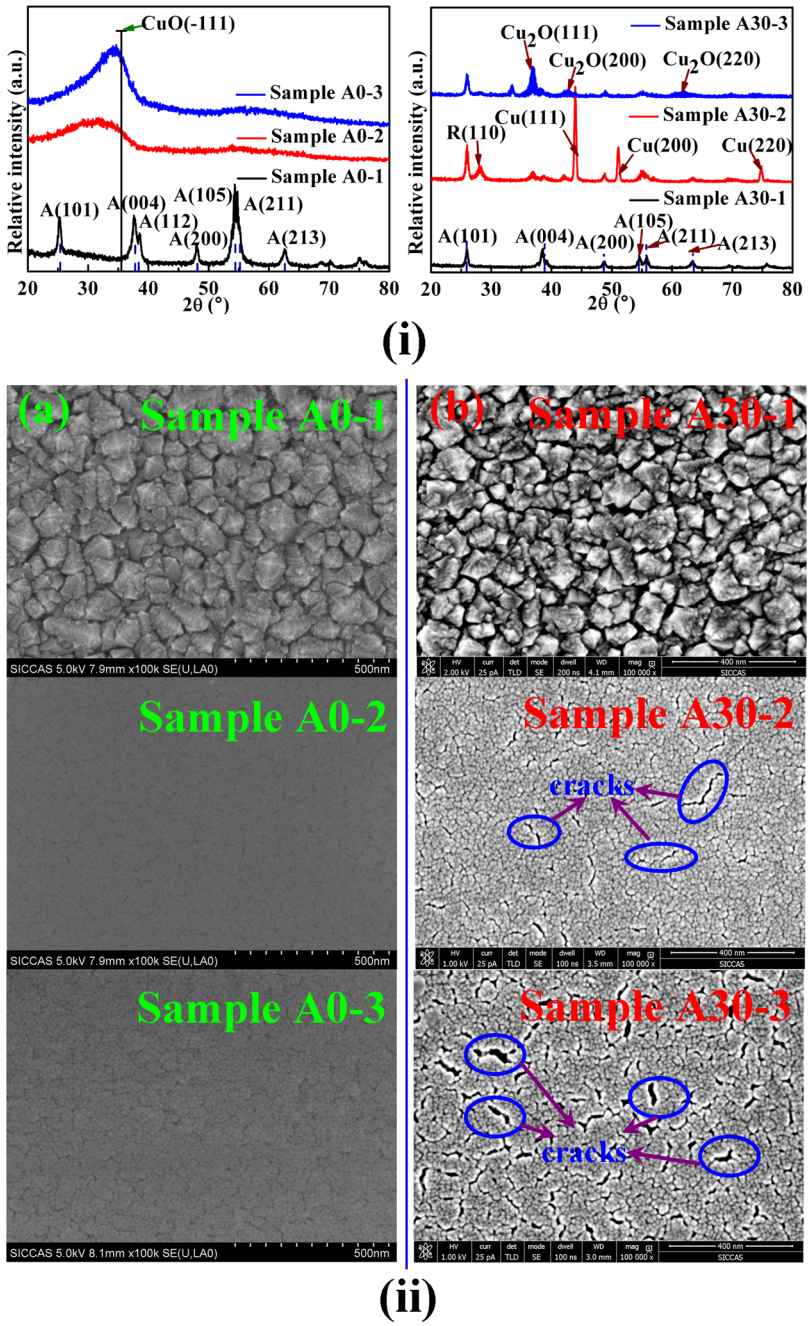

Figure 1. (i) XRD patterns for Cu-doped TiO_2 films at different doping concentration both before and after annealing. The peaks arising from anatase and rutile TiO_2 are indicated by "A" and "R", respectively. (ii) Top view FESEM images of the Cu-doped TiO_2 films: (a) the as-deposited samples, (b) the annealed samples.

Figure 1(i), Sample A30-2 principally contained anatase, CuO, Cu_2O, and rutile phases, while Sample A30-3 only showed some typical peaks of anatase and Cu_2O phases. With respect to generating the Cu metal in Sample A30-2, two crucial factors should be taken into account: (1) low-energy Cu atoms during the deposition and (2) the mobility of nanoparticles in the recrystallization by appropriate annealing temperature. Top view FESEM images (in Figure 1(ii)) of both as-deposited and annealed films demonstrate the influence of doping concentration and postprocessing on the surface topography. In Samples A0-1 and A30-1, the surface morphology was relatively rough and uneven with well-defined prismatic crystals. The root-mean-square (RMS) roughnesses (shown in SI S4) of Samples A0-1 and A30-1 were about 7.9 and 8.5 nm, respectively. And yet, Samples A0-2 and A0-3 only consisted of very fine particles and showed smooth and flat surface with RMS less than 1.9 nm. As mentioned above, excessive Cu dopants in the TiO_2 films give rise to nanocrystalline mixed oxides (e.g., Cu_2O and TiO_2). After annealing at 400 °C, Samples A30-2 and A30-3 were still flat (RMS < 1.7 nm), but their surface yielded evident microcracks, the number of which increased with increasing the doping concentration. In fact, the metastable nanocrystalline mixed oxides are promptly separated and grown into several kinds of big grains (such as Cu_2O, TiO_2, or Cu) by annealing. Meanwhile, the shrinkage stress develops between these grains, and finally the microcracks are caused for the relief of stress. In addition, the

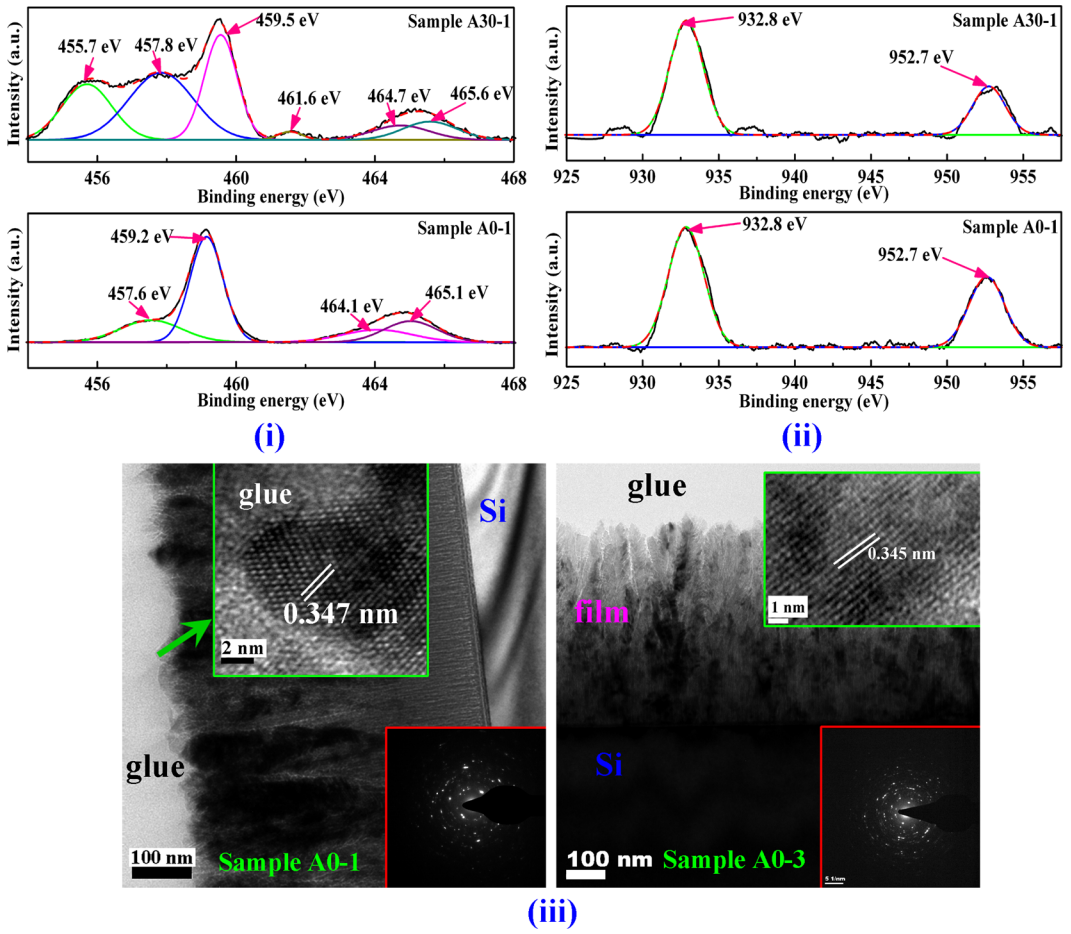

Figure 2. XPS spectra of Ti 2p (i) and Cu 2p (ii) of film surface for Samples A0-1 (bottom) and A30-1 (top), respectively. (iii) Cross-sectional HRTEM images of Samples A0-1 (left) and A30-1 (right), respectively. The upper insets are the high magnification images, and the lower insets show the corresponding fast Fourier transform (FFT).

loose and fissured structure in Samples A30-2 and A30-3 was also observed from the cross-sectional FESEM images (shown in SI S5). The film thicknesses of Samples A0-1, A0-2, and A0-3 in Table 1 were estimated as 502 nm, 512, and 786 nm via FESEM technology, respectively, however, these values were constant even if annealing at 400 °C. Besides, the microstructure of the films was also determined by cross-sectional HRTEM. It is observed that Samples A0-1 and A30-1 (in Figure 2(iii)) only had anatase phase with densed columnar crystal, whereas except anatase phase Samples A0-2 and A0-3 (shown in SI S6 and S7) had the second phase with irregular and tiny grains, which were grown and separated by annealing treatment bringing about the existence of the cracks in the doped films.

To further check if there are the second phase (e.g., Cu, CuO, and Cu_2O) and oxygen defects in Samples A0-1 and A30-1, XPS, and Electron paramagnetic resonance (EPR) experiments were carried out. Figure 2(i) is typical XPS spectra of Ti 2p of Samples A0-1 and A30-1. It is briefly outlined that the Ti $2p_{3/2}$ peak of Samples A30-1 and A0-1 was broader at lower binding energy than that of the TiO_2 films reported by previous work.[25,26] As proposed by Wang et al.,[27] the broadening of Ti $2p_{3/2}$ peak at low binding energy could be ascribed to the appearance of Ti^{3+} or Ti^{2+}. After performing the deconvolution with Lorentzian−Gaussian distribution function, the Ti $2p_{3/2}$ spectrum of Sample A0-1 displayed two peaks at 459.2 and 457.6 eV, which are assigned to Ti^{4+} and Ti^{3+}.[28,29] Nevertheless, except for two peaks at 459.5 eV (Ti^{4+})[30] and 457.8 eV (Ti^{3+}), Sample A30-1 had a 455.7 eV peak in Ti $2p_{3/2}$ spectrum corresponding to Ti^{2+}.[31] It can be indicated that Sample A0-1 and Sample A30-1 possess a certain amount of oxygen vacancies, and the latter shows more significant nonstoichiometric TiO_2 than the former. Actually, ab initio calculations have predicted low vacancy formation energy in the TiO_2 films where there are Cu impurities.[21] Furthermore, XPS spectra of Cu 2p of Samples A0-1 and A30-1 are shown in Figure 2(ii). Samples A0-1 and A30-1 both exhibited the peaks at 932.8 and 952.7 eV, which corresponded to the binding energy of Cu $2p_{3/2}$ and Cu $2p_{1/2}$, respectively. This result is evidently different from that of metallic Cu, which shows Cu $2p_{3/2}$ at 932.3 eV,[32] and simultaneously excludes the possibility of the CuO and Cu_2O cluster formation because the Cu $2p_{3/2}$ core levels for CuO and Cu_2O locate at 933.4 and 932.2 eV, respectively.[33,34] At least, the state points to a considerable fraction of Cu atoms replacing Ti atoms in the host, as studied by X-ray absorption spectroscopy.[35] In addition, low-temperature EPR spectra were also conducted to indentify a certain amount of Ti^{3+} existing in the inner of Samples A0-1 and A30-1, as shown in SI S8. It is well-known that the major feature in this spectrum (g = 1.970 and 1.964 for Samples A0-1 and A30-1, respectively) belongs to the paramagnetic Ti^{3+} centers.[36,37] The EPR signal of Ti^{3+} for Sample A30-1 was more intense than for Sample A0-1, which can be related to more Ti^{3+} or oxygen vacancies existing in Sample A30-1. On the basis of these results, the presence of plentiful oxygen vacancies is unambiguously verified in the inner of Sample A30-1. However, the Cu^{1+}-related EPR signal for

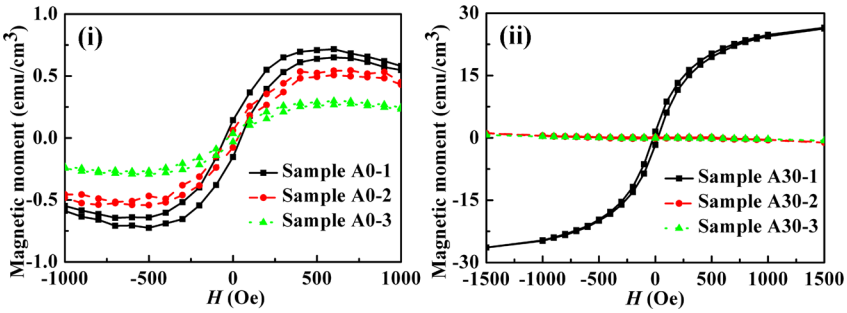

Figure 3. Room-temperature hysteresis curve of as-deposited (i) and annealed (ii) Cu-doped TiO_2 films.

Sample A0-1 and A30-1 was hardly observed at g = 2.00−2.08 (which is assigned to a paramagnetic Cu^{1+} center). As a result, the Cu atoms for Samples A0-1 and A30-1 are only divalent Cu ions to replace Ti atoms in the host. TEM images of Samples A0-1 and A30-1 in Figure 2(iii) showed a dense and continuous columnar structure and the identical film thickness with around 502 nm. For the both samples, the lattice fringes with spacing of 0.347 and 0.345 nm were only assigned to the (101) plane of anatase TiO_2. But anyway, it is revealed from the bottom-right insets in Figure 2(iii) that Samples A0-1 and A30-1 presented a polycrystalline structure consisting of (101), (004), and (105) planes, in accordance with XRD data. In general, the relevant defects mentioned above might lie in the numerous grain boundaries.[38]

Figure 3 shows the magnetization versus magnetic field hysteresis loops for the Cu-doped TiO_2 films. All films were usually measured within one month of preparation because the magnetic moments of the films were unstable over extended periods of time (shown in SI S9). The magnetization data (in Table 1 and Figure 3(i)) collected for Sample A0-1 consistently demonstrated a clear ferromagnetic behavior, with an apparent ferromagnetic M_s of 0.564 emu/cm^3, H_c of 47 Oe, and M_r of 0.144 emu/cm^3. However, the M_s, H_c, and M_r decreased with increasing the amount of Cu. The M_s of Samples A0-2 and A0-3 was calculated to be about 0.441 and 0.240 emu/cm^3, respectively, displaying weak but distinct evidence of magnetic ordering. Although small, this magnetic ordering is of fundamental importance, which declares that the ferromagnetism in the doped TiO_2 films does not come from magnetic impurities. In addition, three reasons can be considered to explain the observation that Cu-doped TiO_2 films with a low doping concentration have high M_s. First, it can be directly related to the distance of the Cu atoms. With increasing doping concentration, the distance between the Cu atoms decreases. In a previous work, Weissmann et al.[39] have indicated that an increased number of Cu atoms occupying adjacent cation lattice positions could result in antiferromagnetic alignment. Therefore, the competition between the ferromagnetism and antiferromagnetism leads to the decrease of M_s with increasing doping concentration. Second, the crystallinity of the Cu-doped TiO_2 films would be one of the effect factor for the variation of the ferromagnetism.[14] For instance, Samples A0-2 and A0-3 are poor in crystal structure, while Sample A0-1 has an excellent crystal structure with well-defined prismatic grains. The improved crystallinity of the films increases the probability of generating impurity band, resulting in greater M_s.[15,40,41] Finally, the ferromagnetism will be weakened if the copper oxide or metal copper is as the second phase in the doped TiO_2 films. Due to its nonferromagnetic properties, the second phase perturbs the presence of magnetic ordering structure in the films. The pinning of the magnetic domains in Samples A0-2 and A0-3 might also be responsible for the low saturation magnetization. However, in this work, these factors are not finally converting the Cu-doped TiO_2 films from the ferromagnetic state to the paramagnetic state.

After vacuum annealing at 400 °C, the 300 K ferromagnetic M_s for Sample A30-1 (in Figure 3(ii)) was 26.41 emu/cm^3 with H_c of 19 Oe and M_r of 1.517 emu/cm^3. Thereinto, the M_s value of Sample A30-1 was around 47 times larger than that of Sample A0-1. From M_s value, we estimate an atomic moment of 47.4 μ_B/Cu in Sample A30-1, assuming 0.19 at. % of Cu and a 502 nm film thickness. However, there is no reason to associate the large moment exclusively with copper, as the high moment (30 μ_B/Co) in the HfO_2 films with the low cobalt doping (0.5 at. %) is expounded.[40] The magnetization in Cu-doped TiO_2 film therefore makes up of a minor component from the transition-metal ion not expected to exceed its spin-only value (1.5 μ_B/Cu),[21] and a major component which can be thought to originate from lattice defects.[42] In general, the two components are oppositely aligned in the dilute limit.[43,44] On the basis of the XRD data, such a small difference of the crystalline between Sample A0-1 and A30-1 can hardly generate enormous difference in their M_s values. The most important factor for enhancing ferromagnetism can be attributed to greater concentration of oxygen vacancies created by vacuum annealing,[45] as elaborated in XPS and EPR section. Assuming a magnetic moment of order 1 μ_B per defect, the vacancy concentration in Sample A30-1 is ∼9 at. %. Moreover, surprisingly, Samples A30-2 and A30-3 had no evidence of magnetic ordering whatsoever, and only showed slight paramagnetism, as depicted in Figure 3(ii). Compared with Samples A0-2 and A0-3, Sample A30-2 and A30-3 showed the distinct microcracks in the films, which forced the crystals to isolate each other and be passivated. The phenomenon can manifest the great mass of oxygen defects at interfacial boundaries between adjacent crystals. Namely, the primary mechanism of ferromagnetism in our Cu-doped TiO_2 films is correlated with interfacial defect formation during deposition.

The proposed activation (or deactivation) and enhancement processes of room-temperature ferromagnetism in the Cu-doped TiO_2 films are summarized in Figure 4(i). As mentioned above, the deposition process produces interfacial defects whose radii are sufficiently large to overlap many adjacent defects, causing a net alignment of defect spins following the BMP mechanism. Additional vacuum annealing treatment passivates the interfacial defects of the films with high doping concentration, transforming the films from ferromagnetism into paramagnetism. But after vacuum annealing, the Cu-doped TiO_2 film with low doping concentration shows even stronger ferromagnetism, owing to the creation of defects. Thus, the magnetic moments arise from atomic point defects in anatase TiO_2 films. Each O site in anatase TiO_2 is surrounded by three Ti ions with one long bond and two

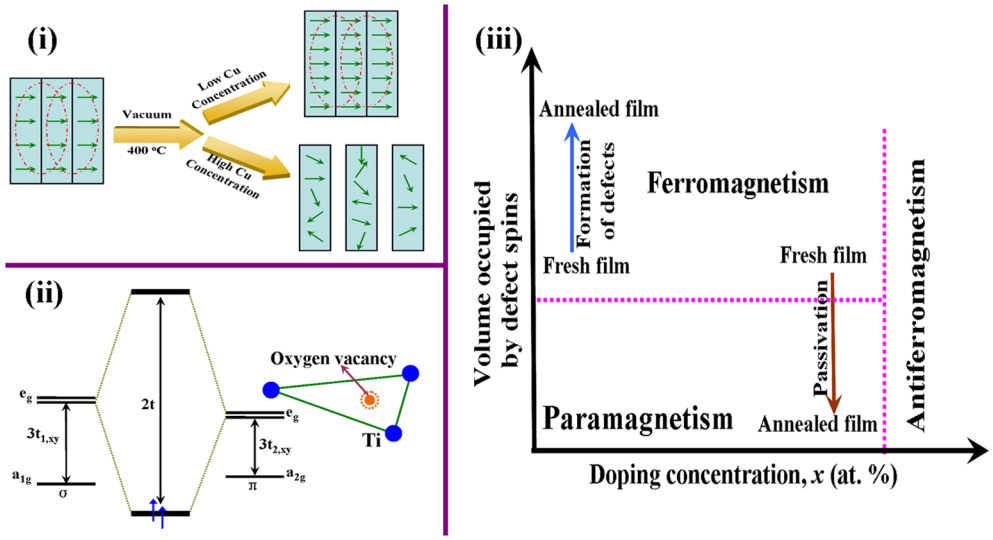

Figure 4. (i) The proposed activation (or deactivation) and enhancement process of room-temperature ferromagnetism. (ii) Schematic diagram for formation of molecular orbitals around an oxygen vacancy in TiO_2 coordinated by three titanium ions. (iii) A magnetic phase diagram (adapted from ref 15) in which the volume occupied by defect spins is plotted versus the doping concentration (x).

short bonds, lying in the same plane.[46] The molecular orbitals are formed from the valence electrons on the three Ti ions surrounding the vacancy via the loss of O ion, as shown in Figure 4(ii). These have σ or π symmetry with respect to the Ti—[O] bond axis, where [O] represents the vacant oxygen site. The σ-bonding orbitals form the symmetries a_{1g} and e_g orbtials and have energies $\varepsilon - 2t_{1,xy}$ and $\varepsilon + t_{1,xy}$, respectively, via a Ti—Ti transfer integral $t_{1,xy}$ orbitals. Similarly, for the π-bonding orbitals with transfer integral $t_{2,xy}$ and t_z orbitals of a_{2g}, e_g, a_{2g}', and e_g' symmetries are formed at $\varepsilon - 2t_{2,xy}$, $\varepsilon + t_{2,xy}$, $\varepsilon - 2t_z$, and $\varepsilon + t_z$, respectively. Only the σ and π orbitals of e_g symmetry will mix, giving bonding and antibonding states with a splitting $2t$, as described in Figure 4(ii). Provided $t > t_{2,xy}$, it is possible for the ring of charge orbital formed from the e_g orbitals to be stabilized relative to the symmetric a_{1g} state.[40,41] Furthermore, since the orbital is degenerate, it can accept two electrons of the same spin, giving a spin moment of 2 μ_B. Provided sufficient defect concentration, the defect-related molecular orbitals will create an impurity band.[15] Direct exchange between the molecular orbitals will be ferromagnetic and can be strong when the defects are concentrated in an interface zone. In addition, Figure 4(iii) displays a magnetic phase diagram (adapted from ref 15) in which the volume occupied by defect spins is plotted versus the doping concentration (x). The volume occupied by defect spins is equal to the volumetric extent of the defect hydrogenic wave function (γ^3) multiplied by the nonstoichiometric defect concentration (δ). Since γ^3 is constant for a given defect and x is constant for a certain film made from fixed deposition conditions, the only parameter varied in the annealing experiments is δ. By regulating the formation (or increase) and passivation of defect in the interface between adjacent crystals, the ferromagnetism is controllably enhanced and turned off.

4. CONCLUSIONS

We have demonstrated that the most important factor for activating ferromagnetism in the Cu-doped TiO_2 films is the creation of bound magnetic polarons, proposed to be oxygen defects in the interface between the adjacent grains. In the case of our experiments, these defects can be increased or passivated, and the ferromagnetism enhanced or destroyed by further vacuum annealing. However, we emphasize that its crystalline nature, second phase, and doping concentration are not the critical factors contributing to the conversion of the films from ferromagnetism and paramagnetism. The present results suggest a path toward the microscopic origins of room-temperature ferromagnetism, drawing particular attention to yielding the nonstoichiometric grain boundary defects in the TiO_2 based DMS materials for their application.

■ ASSOCIATED CONTENT

Supporting Information

Detailed sample preparation, characterization, test methods, and structure of the samples. This material is available free of charge via the Internet at http://pubs.acs.org.

■ AUTHOR INFORMATION

Corresponding Author

*E-mail: p-jin@mail.sic.ac.cn.

Notes

The authors declare no competing financial interest.

■ ACKNOWLEDGMENTS

The authors are grateful to the high-tech project of MOST (2014AA032802), the national sci-tech support plan, the National Natural Science Foundation of China (NSFC, Nos.: 51032008, 51102270, and 51272271).

■ REFERENCES

(1) Jaffe, J. E.; Droubay, T. C.; Chambers, S. A. Oxygen Vacancies and Ferromagnetism in $Co_xTi_{1-x}O_{2-x-y}$. *J. Appl. Phys.* **2005**, *97*, 073908.
(2) Liu, R.; Ke, S. H.; Baranger, H. U.; Yang, W. T. Organometallic Spintronics: Dicobaltocene Switch. *Nano Lett.* **2005**, *5*, 1959−1962.
(3) Matsumoto, Y. Room-Temperature Ferromagnetism in Transparent Transition Metal-Doped Titanium Dioxide. *Science* **2001**, *291*, 854−856.
(4) Bryan, J. D.; Heald, S. M.; Chambers, S. A.; Gamelin, D. R. Strong Room-Temperature Ferromagnetism in Co^{2+}-doped TiO_2 Made from Colloidal Nanocrystals. *J. Am. Chem. Soc.* **2004**, *126*, 11640−11647.
(5) Ruster, C.; Borzenko, T.; Gould, C.; Schmidt, G.; Molenkamp, L. W.; Liu, X.; Wojtowicz, T. J.; Furdyna, J. K.; Yu, Z. G.; Flatte, M. E. Very

Large Magnetoresistance in Lateral Ferromagnetic (Ga,Mn) As Wires with Nanoconstrictions. *Phys. Rev. Lett.* **2003**, *91*, 216602.
(6) Fiederling, R.; Keim, M.; Reuscher, G.; Ossau, W.; Schmidt, G.; Waag, A.; Molenkamp, L. W. Injection and Detection of a Spin-Polarized Current in a Light-Emitting Diode. *Nature* **1999**, *402*, 787–790.
(7) Jonker, B. T.; Park, Y. D.; Bennett, B. R.; Cheong, H. D.; Kioseoglou, G.; Petrou, A. Robust Electrical Spin Injection into a Semiconductor Heterostructure. *Phys. Rev. B* **2000**, *62*, 8180–8183.
(8) Ohno, H.; Chiba, D.; Matsukura, F.; Omiya, T.; Abe, E.; Dietl, T.; Ohno, Y.; Ohtani, K. Electric-Field Control of Ferromagnetism. *Nature* **2000**, *408*, 944–946.
(9) Ohno, H.; Shen, A.; Matsukura, F.; Oiwa, A.; Endo, A.; Katsumoto, S.; Iye, Y. (Ga,Mn)As: A New Diluted Magnetic Semiconductor Based on GaAs. *Appl. Phys. Lett.* **1996**, *69*, 363–365.
(10) Kim, D. H.; Yang, J. S.; Lee, K. W.; Bu, S. D.; Noh, T. W.; Oh, S. J.; Kim, Y. W.; Chung, J. S.; Tanaka, H.; Lee, H. Y.; Kawai, T. Formation of Co Nanoclusters in Epitaxial $Ti_{0.96}Co_{0.04}O_2$ Thin films and Their Ferromagnetism. *Appl. Phys. Lett.* **2002**, *81*, 2421–2423.
(11) Chambers, S. A.; Droubay, T.; Wang, C. M.; Lea, A. S.; Farrow, R. F. C.; Folks, L.; Deline, V.; Anders, S. Clusters and Magnetism in Epitaxial Co-Doped TiO_2 Anatase. *Appl. Phys. Lett.* **2003**, *82*, 1257–1259.
(12) Kim, J. Y.; Park, J. H.; Park, B. G.; Noh, H. J.; Oh, S. J.; Yang, J. S.; Kim, D. H.; Bu, S. D.; Noh, T. W.; Lin, H. J.; Hsieh, H. H.; Chen, C. T. Ferromagnetism Induced by Clustered Co in Co-Doped Anatase TiO_2 Thin Films. *Phys. Rev. Lett.* **2003**, *90*, 017401.
(13) Ye, L. H.; Freeman, A. Defect Compensation, Clustering, and Magnetism in Cr-Doped Anatase TiO_2. *Phys. Rev. B* **2006**, *73*, 081304.
(14) Griffin, K. A.; Pakhomov, A. B.; Wang, C. M.; Heald, S. M.; Krishnan, K. M. Intrinsic Ferromagnetism in Insulating Cobalt Doped Anatase TiO_2. *Phys. Rev. Lett.* **2005**, *94*, 157204.
(15) Coey, J. M. D.; Venkatesan, M.; Fitzgerald, C. B. Donor Impurity Band Exchange in Dilute Ferromagnetic Oxides. *Nat. Mater.* **2005**, *4*, 173–179.
(16) Bryan, J. D.; Santangelo, S. A.; Keveren, S. C.; Gamelin, D. R. Activation of High-T_c Ferromagnetism in Co^{2+}:TiO_2 and Cr^{3+}:TiO_2 Nanorods and Nanocrystals by Grain Boundary Defects. *J. Am. Chem. Soc.* **2005**, *127*, 15568–15574.
(17) Hou, D. L.; Zhao, R. B.; Meng, H. J.; Jia, L. Y.; Ye, X. J.; Zhou, H. J.; Li, X. L. Room-Temperature Ferromagnetism in Cu-Doped TiO_2 Thin Films. *Thin Solid Films* **2008**, *516*, 3223–3226.
(18) Torres, C. E. R.; Golmar, F.; Cabrera, A. F.; Errico, L.; Navarro, A. M. M.; Rentería, M.; Sánchez, F. H.; Duhalde, S. Magnetic and Structural Study of Cu-Doped TiO_2 Thin Films. *Appl. Surf. Sci.* **2007**, *254*, 365–367.
(19) You, M.; Kim, T. G.; Sung, Y.-M. Synthesis of Cu-Doped TiO_2 Nanorods with Various Aspect Ratios and Dopant Concentrations. *Cryst. Growth Des.* **2010**, *10*, 983–987.
(20) Herng, T. S.; Lau, S. P.; Yu, S. F.; Yang, H. Y.; Ji, X. H.; Chen, J. S.; Yasui, N.; Inaba, H. Origin of Room Temperature Ferromagnetism in ZnO:Cu Films. *J. Appl. Phys.* **2006**, *99*, 086101.
(21) Duhalde, S.; Vignolo, M.; Golmar, F.; Chiliotte, C.; Torres, C.; Errico, L.; Cabrera, A.; Rentería, M.; Sánchez, F.; Weissmann, M. Appearance of Room-Temperature Ferromagnetism in Cu-Doped $TiO_{2-\delta}$ Films. *Phys. Rev. B* **2005**, *72*, 161313.
(22) Cromer, D. T.; Herrington, K. The Structures of Anatase and Rutile. *J. Am. Chem. Soc.* **1955**, *77*, 4708–4709.
(23) Hou, D. L.; Meng, H. J.; Jia, L. Y.; Ye, X. J.; Zhou, H. J.; Li, X. L. Impurity Concentration Study on Ferromagnetism in Cu-Doped TiO_2 Thin Films. *Europhys. Lett.* **2007**, *78*, 67001.
(24) Zheng, J. Y.; Hao, J. Y.; Liu, X. Q.; Gong, Q. Y.; Liu, W. M. The Plasma Nitriding Treatment of TiN/TiCN Multilayer Films. *Appl. Surf. Sci.* **2013**, *268*, 195–203.
(25) Wang, Y.; Sun, H. J.; Tan, S. J.; Feng, H.; Cheng, Z. W.; Zhao, J.; Zhao, A. D.; Wang, B.; Luo, Y.; Yang, J. L.; Hou, J. G. Role of Point Defects on the Reactivity of Reconstructed Anatase Titanium Dioxide (001) Surface. *Nat. Commun.* **2013**, *4*, 2214.
(26) Zheng, J. Y.; Bao, S. H.; Guo, Y.; Jin, P. Natural Hydrophobicity and Reversible Wettability Conversion of Flat Anatase TiO_2 Thin Film. *ACS Appl. Mater. Interfaces* **2014**, *6*, 1351–1355.
(27) Wang, L. Q.; Ferris, K. F.; Skiba, P. X.; Shultz, A. N.; Baer, D. R.; Engelhard, M. H. Interactions of Liquid and Vapor Water with Stoichiometric and Defective TiO_2 (100) Surfaces. *Surf. Sci.* **1999**, *440*, 60–68.
(28) Murata, M.; Wakino, K.; Ikeda, S. X-Ray Photoelectron Spectroscopic Study of Perovskite Titanates and Related Compounds—Example of Effect of Polarization on Chemical-Shifts. *J. Electron Spectrosc. Relat. Phenom.* **1975**, *6*, 459–464.
(29) Werfel, F.; Brummer, O. Corundum Structure Oxides Studied by XPS. *Phys. Scr.* **1983**, *28*, 92–96.
(30) Chashechnikova, I. T.; Vorotyntsev, V. M.; Borovik, V. V.; Golodets, G. I.; Plyuto, I. V.; Shpak, A. P. The Nature of Strong Metal-Carrier Interaction in Co Hydrogenation Cobalt-Titanium and Nickel-Titanium Dioxide Catalysts. *Teor. Eksp. Khim.* **1992**, *28*, 216–219.
(31) Franzen, H. F.; Umana, M. X.; Mccreary, J. R.; Thorn, R. J. XPS Spectra of Some Transition-Metal and Alkaline-Earth Monochalcogenides. *J. Solid State Chem.* **1976**, *18*, 363–368.
(32) Strohmeier, B. R.; Leyden, D. E.; Field, R. S.; Hercules, D. M. Surface Spectroscopic Characterization of Cu/Al_2O_3 Catalysts. *J. Catal.* **1985**, *94*, 514–530.
(33) Robert, T.; Offergel, G. X-Ray Photoelectron Spectra of Solid Copper Compounds—Relation between Presence of Satellite Lines and State of Copper Oxidation. *Phys. Status Solidi A* **1972**, *14*, 277–282.
(34) Nakai, I.; Sugitani, Y.; Nagashima, K.; Niwa, Y. X-Ray Photoelectron Spectroscopic Study of Copper Minerals. *J. Inorg. Nucl. Chem.* **1978**, *40*, 789–791.
(35) Torres, C. E. R.; Cabrera, A. F.; Errico, L. A.; Duhalde, S.; Renteria, M.; Golmar, F.; Sanchez, F. H. XAS Study of the Local Environment of Impurities in Doped TiO_2 Thin Films. *Phys. B* **2007**, *398*, 219–222.
(36) Yu, X.; Kim, B.; Kim, Y. K. Highly Enhanced Photoactivity of Anatase TiO_2 Nanocrystals by Controlled Hydrogenation-Induced Surface Defects. *ACS Catal.* **2013**, 3 (11), 2479–2486.
(37) Zuo, F.; Wang, L.; Wu, T.; Zhang, Z. Y.; Borchardt, D.; Feng, P. Y. Self-Doped Ti^{3+} Enhanced Photocatalyst for Hydrogen Production under Visible Light. *J. Am. Chem. Soc.* **2010**, *132* (34), 11856–11857.
(38) Coey, J. M. D. High-Temperature Ferromagnetism in Dilute Magnetic Oxides. *J. Appl. Phys.* **2005**, *97*, 10D313.
(39) Weissmann, M.; Errico, L. A. The Role of Vacancies, Impurities and Crystal Structure in the Magnetic Properties of TiO_2. *Phys. B* **2007**, *398*, 179–183.
(40) Coey, J.; Venkatesan, M.; Stamenov, P.; Fitzgerald, C.; Dorneles, L. Magnetism in Hafnium Dioxide. *Phys. Rev. B* **2005**, *72*, 024450.
(41) Elfimov, I.; Yunoki, S.; Sawatzky, G. Possible Path to a New Class of Ferromagnetic and Half-Metallic Ferromagnetic Materials. *Phys. Rev. Lett.* **2002**, *89*, 216403.
(42) Venkatesan, M.; Fitzgerald, C. B.; Coey, J. M. D. Unexpected Magnetism in a Dielectric Oxide. *Nature* **2004**, *430*, 630.
(43) Kaminski, A.; Das Sarma, S. Polaron Percolation in Diluted Magnetic Semiconductors. *Phys. Rev. Lett.* **2002**, *88*, 247202.
(44) Wolff, P. A.; Bhatt, R. N.; Durst, A. C. Polaron–Polaron Interactions in Diluted Magnetic Semiconductors. *J. Appl. Phys.* **1996**, *79*, 5196–5198.
(45) Foster, A. S.; Gejo, F. L.; Shluger, A. L.; Nieminen, R. M. Vacancy and Interstitial Defects in Hafnia. *Phys. Rev. B* **2002**, *65*, 174117.
(46) Lazzeri, M.; Vittadini, A.; Selloni, A. Structure and Energetics of Stoichiometric TiO_2 Anatase Surfaces. *Phys. Rev. B* **2001**, *63*, 155409.